Vietnam Journal of Agricultural Sciences

p-ISSN 2588-1299
e-ISSN 3030-4520

VJAS 2025; 8(2): 2493-2508
https://doi.org/10.31817/vjas.2025.8.2.06

Free Vibration Analysis of Sandwich Plates with Auxetic Core and Porous FGM Faces Resting on Winkler/Pasternak/Kerr Elastic Foundations

Dao Cong Binh[1], Duong Thanh Huan[2*], Nguyen Thanh Hai[2], Le Vu Quan[2], Luong Thi Minh Chau[2] & Hoang Xuan Anh[2]

[1]Institute of Techniques for Special Engineering, Le Quy Don Technical University, Hanoi 11900, Vietnam

[2]Faculty of Engineering, Vietnam National University of Agriculture, Hanoi 12400, Vietnam

Abstract

The paper presents an analytical solution to investigate the free vibration of a sandwich plate with an auxetic core (negative Poisson's ratio) and functionally graded face sheets containing porosities (PoFGM), based on the four-variable higher-order shear deformation theory (HSDT-4). The plate is assumed to be supported by Winkler, Pasternak, or Kerr elastic foundations. The governing equations were derived using Hamilton's principle and were solved analytically using the Navier solution for a rectangular plate with simply supported edges. The results were validated through comparisons with previously published studies, demonstrating the accuracy and reliability of the proposed approach. In addition, the effects of material properties (porosity distribution patterns, porosity volume fraction), geometric parameters of the auxetic core unit cell, the geometric dimensions of the plate, and the elastic foundation on the vibration characteristics were thoroughly analyzed.

Keywords

Free vibration analysis, sandwich plates, FGM, porosity, auxetic, elastic foundations

Introduction

Functionally graded materials (FGMs), as a new class of materials composed of two or more components, exhibit smooth and continuous variation in properties along defined directions. With their outstanding advantages, FGMs enable optimal mechanical design and effectively address the delamination issues commonly encountered in traditional composite materials. FGMs can be fabricated from a variety of materials, primarily metals and ceramics. Ceramics contribute heat resistance, while metals enhance strength

Received: April 21, 2025
Accepted: June 15, 2025

Correspondence to
Duong Thanh Huan
dthuan@vnua.edu.vn

ORCID
Duong Thanh Huan
https://orcid.org/0000-0002-2045-7759

and ductility, making FGMs particularly suitable for components operating in high-temperature environments (Reddy, 2000; Zenkour, 2006; Zhao & Liew, 2009).

Sandwich plates made from functionally graded materials have evolved into advanced structural systems due to their ability to combine diverse material characteristics within a single configuration. These plates are often engineered with components that vary through the thickness, enhancing properties such as strength-to-weight ratio, thermal resistance, and impact resistance. Consequently, they are widely applied in demanding engineering sectors, including automotive, marine, nuclear, aviation, and aerospace industries. To better understand their behavior, researchers have conducted numerous studies using different shear deformation theories. For example, Thai *et al*. (2014) proposed an improved first-order plate theory to analyze the bending, stability, and free vibration characteristics of FGM-based sandwich plates. Zenkour (2005a; 2005b) introduced a generalized higher-order shear deformation theory (HSDT) to investigate the mechanical behavior of functionally graded plates. Houari *et al.* (2013) applied a modified HSDT to study the thermoelastic bending of FGM sandwich plates, while Alibeigloo & Alizadeh (2015) used three-dimensional elasticity theory to examine their static and dynamic responses.

Modern advanced materials such as composite materials, FGMs, porous materials, and piezoelectric materials- typically exhibit positive Poisson's ratios. This means they contract laterally when subjected to tensile forces and expand laterally under compressive forces. In contrast, auxetic materials (Alderson & Evans, 1995), which are a class of advanced materials with negative Poisson's ratios, have attracted considerable attention due to their unique and superior properties, including low weight, high stiffness-to-weight ratio, excellent sound and thermal insulation, and outstanding energy absorption capabilities. Sandwich plates with auxetic cores show significant potential for military applications, such as forming mats that enable military vehicles and armored personnel carriers to traverse soft or swampy terrain. Moreover, such structures can serve as protective armor, reducing overall weight while improving acoustic insulation, thermal resistance, and impact mitigation against collisions or shock waves from explosions (Ghazwani *et al*., 2024). Tran *et al.* (2020) investigated the dynamic response of sandwich plates with auxetic honeycomb cores resting on elastic foundations under moving loads. Imbalzano *et al*. (2016) analyzed the dynamic behavior of auxetic composite plates under explosive loading. Quoc *et al*. (2023) explored the free vibration and nonlinear behavior of composite sandwich plates with auxetic honeycomb cores and piezoelectric face sheets. Nguyen *et al*. (2021) conducted an in-depth study of sandwich plates with auxetic cores subjected to blast loads. Comprehensive insights into auxetic structural analysis, including structural types, materials, analytical methods, and manufacturing techniques, are provided in the review by Bohara *et al.* (2023).

In the manufacturing of FGMs using techniques such as layered infiltration and sintering, porosity often arises within the material structure, significantly affecting its mechanical properties. Numerous studies have been conducted to evaluate the effects of porosity distribution and porosity ratio on the mechanical behavior of porous FGM (Po-FGM) plate structures. Aït Atmane *et al.* (2017) investigated the influence of porosity on the mechanical response of Po-FGM beams resting on elastic foundations. Yousfi *et al.* (2018) analyzed the impact of porosity on the vibration characteristics of FGM plates by applying shear deformation theory with sinusoidal displacement functions and Navier-type solutions. Merdaci *et al*. (2021) examined the natural vibration behavior of Po-FGM plates using a higher-order shear deformation theory in conjunction with the Navier method. Le Thanh Hai *et al.* (2024) studied the natural vibration and dynamic response of Po-FGM sandwich plates placed on a Kerr-type elastic foundation using a simplified first-order shear deformation theory. Liang & Wang (2020) proposed a quasi-3D trigonometric shear deformation theory to investigate wave propagation in Po-FGM sandwich plates resting on a viscoelastic foundation.

Many practical structures such as pipelines, railways, and pontoon bridges are constructed on elastic foundations, making the study of FGM plate structures on such foundations both important and highly relevant. The three commonly used elastic foundation models are the Winkler, Pasternak, and Kerr models. The Winkler model (Winkler, 1867) is the simplest, representing the foundation as a series of independent springs, but it fails to capture the continuity of the foundation. To address this limitation, the Pasternak model (Pasternak, 1954) introduced a shear interaction parameter. Building on both, the Kerr model (1965; 1984) further enhanced the accuracy by incorporating layered spring interactions, offering a more realistic representation of elastic foundations. Kumar & Harsha (2022) applied the First-Order Shear Deformation Theory (FSDT) to investigate the static behavior of piezoelectric Po-FGM sandwich plates placed on Winkler, Pasternak, and Kerr foundations under mechanical, thermal, and electrical loading. Li *et al.* (2021) used the Higher-Order Shear Deformation Theory (HSDT) to study the free vibration of FGM plates on these foundation models. Shahsavari *et al.* (2018) explored the free vibration of Po-FGM plates using three-dimensional elasticity theory with a hyperbolic displacement function, considering all three foundation types. Recent studies (Vu Van Tham *et al.*, 2024; Vu Van Tham, 2025) further demonstrate the increasing use of the Kerr foundation model in vibration analyses of fundamental structural elements such as beams, plates, and shells.

As mentioned above, there have been no prior studies on the free vibration behavior of SAFGP (porous Sandwich Auxetic-FGM plates) structures resting on Winkler, Pasternak, or Kerr foundations. Therefore, it is necessary to fill this research gap and contribute to the development of this field. Beyond its theoretical significance, investigating the vibration characteristics of SAFGP plates on elastic foundations opens up numerous potential applications in engineering structures, especially as the materials used in these plates are gaining increased attention. To address this deficit, this paper proposes an analytical model based on the Higher-Order Shear Deformation Theory (HSDT-4) to study the free vibration of SAFGP plates on Winkler, Pasternak, and Kerr foundations. The results obtained are validated by comparing them with existing literature to confirm the reliability of the proposed model. Building on this foundation, this study further explores the effects of material properties, the porosity distribution and coefficient, auxetic unit cell geometry, plate dimensions, and elastic foundation parameters on the fundamental frequencies of SAFGP plates.

Methods

SAFGP plates resting on Winkler/Pasternak/Kerr elastic foundation

In this study, a sandwich plate with two Po-FGM face layers and an auxetic honeycomb core layer resting on a Winkler/Pasternak/Kerr elastic foundation was considered. The plate dimensions are illustrated in **Figure 1**.

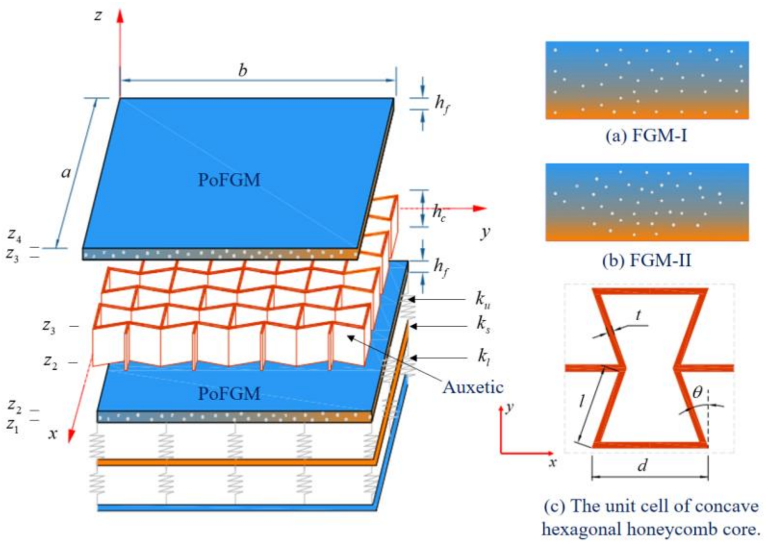

Figure 1. Schematic of sandwich plate with honeycomb core and porous FGM face sheets resting on Kerr foundation

The dimension of SAFGP plate is $a \times b$ and the total thickness is $h = h_c + 2h_f$ where h_c and h_f are the thickness of the core layer and two face layers as shown in **Figure 1**. The PoFGM material consists of ceramic and metal. The effective properties $P^{(L)}$ of each L^{th} layer (L = 1, 2, 3) are assumed to vary smoothly along the thickness of the plate according to a power law as in the followings:

$$P^{(N)}(z) = P_m + \left(P_c - P_m\right)V_c^{(N)} - \frac{\alpha_0}{2}\left(P_c + P_m\right)\delta^{(N)} \tag{1}$$

where N represents the number of layers of the plate; α_0 is the porosity coefficient; P_m and P_c are the material properties of the metal and ceramic, respectively; $V_c^{(L)}$ is the volume fraction of the ceramic and $\delta^{(L)}$ is a step function.

The ceramic volume fraction $V_c^{(L)}$ and step function $\delta^{(L)}$ for three types of sandwich plates SPoFGM-I, SPoFGM-II are defined as follows (Li *et al.*, 2008):

Layer 1 (PoFGM at the bottom of the plate): $V_c(z) = \left(\dfrac{z - z_1}{z_2 - z_1}\right)^p$ with $z \in \left[z_1, z_2\right]$ (2)

Layer 2 (auxetic core layer): calculated according to Equation (7) and $z \in \left[z_2, z_3\right]$ (3)

Layer 3 (PoFGM at the top of the plate): $V_c(z) = \left(\dfrac{z - z_4}{z_3 - z_4}\right)^p$ with $z \in \left[z_3, z_4\right]$ (4)

Uniform porosity distribution type (FGM-I):

$$\delta^{(1)} = \delta^{(3)} = 1 \tag{5}$$

Non-uniform porosity distribution type (FGM-II):

$$\delta^{(1)} = \left(1 - \frac{\left|2z - (z_1 + z_0)\right|}{z_1 - z_0}\right);\ \delta^{(3)} = \left(1 - \frac{\left|2z - (z_3 + z_2)\right|}{z_3 - z_2}\right). \tag{6}$$

For the auxetic honeycomb core, the important geometrical parameters of the structural unit cell are determined and illustrated in **Figure 1(c)**. Equation (7) describes the effective properties of the structure, in which the geometrical parameters d, l, t, θ are defined as the horizontal side length, the inclined side length, the thickness of each characteristic element, and the inclined angle, respectively (Tran *et al.*, 2020).

$$\begin{gathered}
E_1^C = E\frac{\eta_3^3\left(\eta_1 - \sin\theta\right)}{\cos^3\theta\left[1 + \left(\tan^2\theta + \eta_1\sec^2\theta\right)\eta_3^2\right]},\ G_{12}^C = E\frac{\eta_3^3}{\eta_1\cos\theta\left(1 + 2\eta_1\right)}, \\
E_2^C = E\frac{\eta_3^3}{\cos\theta\left(\eta_1 - \sin\theta\right)\left(\tan^2\theta + \eta_3^2\right)},\ G_{23}^C = G\frac{\eta_3\cos\theta}{\eta_1 - \sin\theta}, \\
G_{13}^C = G\frac{\eta_3}{2\cos\theta}\left[\frac{\eta_1 - \sin\theta}{1 + 2\eta_1} + \frac{\eta_1 + 2\sin^2\theta}{2\left(\eta_1 - \sin\theta\right)}\right],\ \rho^C = \rho\frac{\eta_3\left(\eta_1 + 2\right)}{2\cos\theta\left(\eta_1 - \sin\theta\right)}, \\
\nu_{12}^C = -\frac{\sin\theta\left[1 - \eta_3^2\right]\left(\eta_1 - \sin\theta\right)}{\cos^2\theta\left[1 + \left(\tan^2\theta + \eta_1\sec^2\theta\right)\eta_3^2\right]}, \\
\nu_{21}^C = -\frac{\sin\theta\left[1 - \eta_3^2\right]}{\left[\tan^2\theta + \eta_3^2\right]\left(\eta_1 - \sin\theta\right)},\ \eta_1 = \frac{d}{l},\ \eta_3 = \frac{t}{l}.
\end{gathered} \tag{7}$$

Governing equations

To analyze the natural vibration of the SAFGP plate placed on elastic foundation, we utilized the HSDT-4 theory. The displacement field was defined such as Quoc *et al.* (2019):

$$\begin{aligned} u\left(x,y,z,t\right) &= u_0(x,y,t) - z\frac{\partial w_b(x,y,t)}{\partial x} - f\left(z\right)\frac{\partial w_s(x,y,t)}{\partial x};\\ v\left(x,y,z,t\right) &= v_0(x,y,t) - z\frac{\partial w_b(x,y,t)}{\partial y} - f\left(z\right)\frac{\partial w_s(x,y,t)}{\partial y};\\ w\left(x,y,z,t\right) &= w_b(x,y,t) + w_s(x,y,t) \end{aligned} \tag{8}$$

in which w_b and w_s were the deflection components due to bending and due to shear, respectively.; u_0, v_0 were the displacements at the middle surface in the direction x, y; $f(z)$ was the shear stress distribution function along the plate thickness. Following Quoc *et al*. (2019), the function $f\left(z\right) = -z\left(\frac{1}{8} - \frac{3}{2}\left(\frac{z}{h}\right)^2\right)$ satisfies the condition that the transverse shear stress at the top and bottom of the plate is zero.

The strain field was derived from the displacement field as below:

$$\begin{aligned} \varepsilon &= \varepsilon_0 + z\varepsilon_1 + f(z)\varepsilon_2\\ \gamma &= g(z)\gamma_0 \end{aligned} \tag{9}$$

where

$$\begin{aligned} &\varepsilon = \left\{\varepsilon_{xx}\ \ \varepsilon_{yy}\ \ \varepsilon_{xy}\right\}^T; \varepsilon_0 = \left\{\frac{\partial u}{\partial x}\ \ \frac{\partial v}{\partial y}\ \ \frac{\partial u}{\partial y} + \frac{\partial v}{\partial x}\right\}^T;\\ &\varepsilon_1 = -\left\{\frac{\partial^2 w_b}{\partial x^2}\ \ \frac{\partial^2 w_b}{\partial y^2}\ \ 2\frac{\partial w_b}{\partial x\partial y}\right\}^T;\\ &\varepsilon_2 = -\left\{\frac{\partial^2 w_s}{\partial x^2}\ \ \frac{\partial^2 w_s}{\partial y^2}\ \ \frac{2\partial w_s}{\partial x\partial y}\right\}^T;\ \gamma = \left\{\gamma_{xz}\ \ \gamma_{yz}\right\};\\ &\gamma_0 = \left\{\frac{\partial w_s}{\partial x}\ \ \frac{\partial w_s}{\partial y}\right\};\ g(z) = 1 - f^{'}(z) \end{aligned} \tag{10}$$

The stress-strain relationship followed the Hooke's law, which is defined by:

$$\begin{Bmatrix} \sigma_{xx}\\ \sigma_{yy}\\ \sigma_{xy}\\ \sigma_{xz}\\ \sigma_{yz} \end{Bmatrix}^{(k)} = \begin{bmatrix} C_{11} & C_{12} & 0 & 0 & 0\\ C_{12} & C_{11} & 0 & 0 & 0\\ 0 & 0 & C_{66} & 0 & 0\\ 0 & 0 & 0 & C_{44} & 0\\ 0 & 0 & 0 & 0 & C_{55} \end{bmatrix}^{(k)} \begin{Bmatrix} \varepsilon_{xx}\\ \varepsilon_{yy}\\ \gamma_{xy}\\ \gamma_{xz}\\ \gamma_{yz} \end{Bmatrix} \tag{11}$$

in which $k = b$; c; t represented the bottom, core and top layers of the sandwich plate, respectively. For the two PoFGM surface layers:

$$C_{11} = \frac{E(z)}{1-v^2};\ C_{12} = \frac{vE(z)}{1-v^2};\ C_{44} = C_{55} = C_{66} = \frac{E(z)}{2\left(1+v\right)} \tag{12}$$

For the auxetic core layer:

$$C_{11}^{c}=\frac{E_1^{2}}{1-v_{12}^{c}v_{21}^{c}};\quad C_{22}^{c}=\frac{E_2^{c}}{1-v_{12}^{c}v_{21}^{c}};\quad C_{12}^{c}=\frac{v_{12}^{c}E_2^{c}}{1-v_{12}^{c}v_{21}^{c}};\quad C_{21}^{c}=\frac{v_{21}^{c}E_2^{c}}{1-v_{12}^{c}v_{21}^{c}};C_{66}^{c}=G_{12}^{c};$$
$$C_{55}^{c}=G_{13}^{c};\ C_{44}^{c}=G_{23}^{c}\tag{13}$$

Next, we substituted the strain components in Eq. (10) into Eq. (11) and then integrated along the plate thickness to obtain the relationship between the internal force resultants and strains:

$$\begin{Bmatrix} N_x \\ N_y \\ N_{xy} \end{Bmatrix}=\begin{bmatrix} A_{11} & A_{12} & 0 \\ A_{12} & A_{22} & 0 \\ 0 & 0 & A_{66} \end{bmatrix}\begin{Bmatrix} \varepsilon_x^0 \\ \varepsilon_y^0 \\ \gamma_{xy}^0 \end{Bmatrix};$$
$$\begin{Bmatrix} M_x^b \\ M_y^b \\ M_{xy}^b \end{Bmatrix}=\begin{bmatrix} D_{11} & D_{12} & 0 \\ D_{12} & D_{22} & 0 \\ 0 & 0 & D_{66} \end{bmatrix}\begin{Bmatrix} \kappa_x^b \\ \kappa_y^b \\ \kappa_{xy}^b \end{Bmatrix}+\begin{bmatrix} D_{11}^s & D_{12}^s & 0 \\ D_{12}^s & D_{22}^s & 0 \\ 0 & 0 & D_{66}^s \end{bmatrix}\begin{Bmatrix} \kappa_x^s \\ \kappa_y^s \\ \kappa_{xy}^s \end{Bmatrix};$$
$$\begin{Bmatrix} M_x^s \\ M_y^s \\ M_{xy}^s \end{Bmatrix}=\begin{bmatrix} D_{11}^s & D_{12}^s & 0 \\ D_{12}^s & D_{22}^s & 0 \\ 0 & 0 & D_{66}^s \end{bmatrix}\begin{Bmatrix} \kappa_x^b \\ \kappa_y^b \\ \kappa_{xy}^b \end{Bmatrix}+\begin{bmatrix} H_{11}^s & H_{12}^s & 0 \\ H_{12}^s & H_{22}^s & 0 \\ 0 & 0 & H_{66}^s \end{bmatrix}\begin{Bmatrix} \kappa_x^s \\ \kappa_y^s \\ \kappa_{xy}^s \end{Bmatrix};\tag{14}$$
$$\begin{Bmatrix} Q_{yz} \\ Q_{xz} \end{Bmatrix}=\begin{bmatrix} A_{44}^s & 0 \\ 0 & A_{55}^s \end{bmatrix}\begin{Bmatrix} \gamma_{yz}^s \\ \gamma_{xz}^s \end{Bmatrix}$$

in which

$$(A_{ij},D_{ij},D_{ij}^s,H_{ij}^s)=\int_{z_1}^{z_2}(1,z^2,zf(z),f^2(z))C_{ij}dz$$
$$+\int_{z_2}^{z_3}(1,z^2,zf(z),f^2(z))C_{ij}^c(z)dz$$
$$+\int_{z_3}^{z_4}(1,z^2,zf(z),f^2(z))C_{ij}dz;\quad i,j=1,2,3,6;\tag{15}$$
$$A_{ij}^s=\int_{z_1}^{z_2}\left(g(z)\right)^2C_{ij}dz+\int_{z_2}^{z_3}\left(g(z)\right)^2C_{ij}^cdz$$
$$+\int_{z_3}^{z_4}\left(g(z)\right)^2C_{ij}dz;\ i,j=4,5$$

The HSDST-4 equations of motion of the SAFGP plate placed on an elastic foundation were obtained using Hamilton's principle Quoc *et al.* (2019):

$$\delta u_0:\frac{\partial N_x}{\partial x}+\frac{\partial N_{xy}}{\partial y}=I_0\ddot{u}-I_1\frac{\partial \ddot{w}_b}{\partial x}-I_3\frac{\partial \ddot{w}_s}{\partial x}\tag{16}$$
$$\delta v_0:\frac{\partial N_y}{\partial y}+\frac{\partial N_{xy}}{\partial x}=I_0\ddot{v}-I_1\frac{\partial \ddot{w}_b}{\partial y}-I_3\frac{\partial \ddot{w}_s}{\partial y}$$
$$\delta w_b:\frac{\partial^2 M_x^b}{\partial x^2}+2\frac{\partial^2 M_{xy}^b}{\partial x\partial y}+\frac{\partial^2 M_y^b}{\partial y^2}=I_0(\ddot{w}_b+\ddot{w}_s)+I_1(\frac{\partial \ddot{u}}{\partial x}+\frac{\partial \ddot{u}}{\partial y})$$
$$-I_2\nabla^2\ddot{w}_b-I_4\nabla^2\ddot{w}_s$$
$$\delta w_s:\frac{\partial^2 M_x^s}{\partial x^2}+2\frac{\partial^2 M_{xy}^s}{\partial x\partial y}+\frac{\partial^2 M_y^s}{\partial y^2}+\frac{\partial Q_{xz}^s}{\partial x}+\frac{\partial Q_{yz}^s}{\partial y}=I_0(\ddot{w}_b+\ddot{w}_s)$$

$$+I_3\left(\frac{\partial \ddot{u}}{\partial x}+\frac{\partial \ddot{v}}{\partial y}\right)-I_4\nabla^2\ddot{w}_b-I_5\nabla^2\ddot{w}_s$$

in which $\nabla^2=\partial/\partial x^2+\partial/\partial y^2$ was the Laplace operator in rectangular Cartesian coordinates.

Moments of inertia $I_0, I_1, ..., I_5$ were defined as follows:

$$\begin{aligned}\left(I_0,I_1,I_2,I_3,I_4,I_5\right)&=\int_{z_1}^{z_2}\rho_{FG}^b\left(z\right)\left(1,z,f(z),zf(z),z^2,f(z)^2\right)dz\\&+\int_{z_2}^{z_3}\rho^c\left(z\right)\left(1,z,f(z),zf(z),z^2,f(z)^2\right)dz\\&+\int_{z_3}^{z_4}\rho_{FG}^t\left(z\right)\left(1,z,f(z),zf(z),z^2,f(z)^2\right)dz\end{aligned}\tag{17}$$

where $\rho^c, \rho_{FG}^t, \rho_{FG}^b$ were the mass densities of the auxetic core layer, the top PoFGM layer and the bottom PoFGM layer, respectively.

Substituting the internal force resultants in terms of displacements in Eq. (14) into Eq. (16), we obtained the system of equations of motion of the SAFGP plate placed on the Winkler/Pasternak/Kerr elastic foundation in terms of displacements:

$$\begin{aligned}&\delta u_0: A_{11}\frac{\partial^2 u_0}{\partial x^2}+\left(A_{12}+A_{66}\right)\frac{\partial^2 v_0}{\partial x\partial y}+A_{66}\frac{\partial^2 u_0}{\partial y^2}=I_0\ddot{u}-I_1\frac{\partial \ddot{w}_b}{\partial x}-I_3\frac{\partial \ddot{w}_s}{\partial x};\\&\delta v_0: A_{11}\frac{\partial^2 v_0}{\partial y^2}+\left(A_{12}+A_{66}\right)\frac{\partial^2 u_0}{\partial x\partial y}+A_{66}\frac{\partial^2 v_0}{\partial x^2}=I_0\ddot{v}-I_1\frac{\partial \ddot{w}_b}{\partial y}-I_3\frac{\partial \ddot{w}_s}{\partial y};\\&\delta w_b: D_{11}^b\frac{\partial^4 w_b}{\partial x^4}+2\left(D_{12}^b+2D_{66}^b\right)\frac{\partial^4 w_b}{\partial x^2\partial y^2}+D_{22}^b\frac{\partial^4 w_b}{\partial y^4}+D_{11}^s\frac{\partial^4 w_s}{\partial x^4}\\&+2\left(D_{12}^s+2D_{66}^s\right)\frac{\partial^4 w_s}{\partial x^2\partial y^2}+D_{22}^s\frac{\partial^4 w_s}{\partial y^4}-f_e\\&=I_0(\ddot{w}_b+\ddot{w}_s)+I_1\left(\frac{\partial \ddot{u}}{\partial x}+\frac{\partial \ddot{u}}{\partial y}\right)-I_2\nabla^2\ddot{w}_b-I_4\nabla^2\ddot{w}_s;\\&\delta w_s: D_{11}^s\frac{\partial^4 w_b}{\partial x^4}+2\left(D_{12}^s+2D_{66}^s\right)\frac{\partial^4 w_b}{\partial x^2\partial y^2}+D_{22}^s\frac{\partial^4 w_b}{\partial y^4}+H_{11}^s\frac{\partial^4 w_s}{\partial x^4}\\&+2\left(H_{12}^s+2H_{66}^s\right)\frac{\partial^4 w_s}{\partial x^2\partial y^2}+H_{22}^s\frac{\partial^4 w_s}{\partial y^4}-A_{55}^s\frac{\partial^2 w_s}{\partial x^2}-A_{44}^s\frac{\partial^2 w_s}{\partial y^2}\\&-f_e=I_0(\ddot{w}_b+\ddot{w}_s)+I_3\left(\frac{\partial \ddot{u}}{\partial x}+\frac{\partial \ddot{v}}{\partial y}\right)-I_4\nabla^2\ddot{w}_b-I_5\nabla^2\ddot{w}_s\end{aligned}\tag{18}$$

where f_e was the foundation reaction, determined by the following formula (Li *et al*., 2021):

$$\begin{aligned}&f_e=k_w\left(w_b+w_s\right) \text{ for Winkler foundation;}\\&f_e=k_w\left(w_b+w_s\right)-k_p\nabla^2\left(w_b+w_s\right) \text{ for Pasternak foundation;}\\&f_e=\left(k_l k_u\right)/\left(k_l+k_u\right)\left(w_b+w_s\right)-\left(k_s k_u\right)/\left(k_l+k_u\right)\nabla^2\left(w_b+w_s\right) \text{ for Kerr foundation.}\end{aligned}\tag{19}$$

in which k_w k_p were the bending and shear stiffness coefficients of the Winkler-Pasternak foundation; k_l, k_s, k_u was the triplet of the corresponding Kerr stiffness coefficients.

Navier solution

In this study, the free vibration of a SAFGP plate placed on a Winkler/Pasternak/Kerr elastic foundation was analyzed using the Navier solution with simply supported boundary condition (SSSS), expressed as follows:

$$\begin{aligned} &\mathrm{v}_0 = \mathrm{w}_b = \mathrm{w}_s = N_x = M_x = 0 \ \text{, at } x = 0, a \\ &\mathrm{u}_0 = \mathrm{w}_b = \mathrm{w}_s = N_y = M_y = 0 \ \text{, at } y = 0, b \end{aligned} \tag{20}$$

The displacement components were assumed to be in the form of double trigonometric series, satisfying the boundary conditions shown in Eq. (20):

$$\begin{aligned} u_0(x,y,t) &= \sum_{m=1}^{\infty}\sum_{n=1}^{\infty} u_{mn}\, \mathrm{e}^{i\omega t} \cos\alpha x \sin\beta y; \\ v_0(x,y,t) &= \sum_{m=1}^{\infty}\sum_{n=1}^{\infty} v_{mn}\, \mathrm{e}^{i\omega t} \sin\alpha x \cos\beta y; \\ w_b(x,y,t) &= \sum_{m=1}^{\infty}\sum_{n=1}^{\infty} w_{bmn}\, \mathrm{e}^{i\omega t} \sin\alpha x \sin\beta y; \\ w_s(x,y,t) &= \sum_{m=1}^{\infty}\sum_{n=1}^{\infty} w_{smn}\, \mathrm{e}^{i\omega t} \sin\alpha x \sin\beta y. \end{aligned} \tag{21}$$

where $\alpha = m\pi / a,\ \beta = n\pi / b$, ω was the angular fundamental frequency (*rad*/*s*) and the unknown coefficients to be determined were $\{X\} = \{u_{mn},\ v_{mn},\ w_{bmn},\ w_{smn}\}^T$.

Substituting Eq. (21) into Eq. (18) and then perform mathematical manipulations, we obtained the following equation:

$$\left\{[K]_{4\times4} - \omega^2 [M]_{4\times4}\right\}\{X\} = \{0\} \tag{22}$$

with coefficients k_{ij} and m_{ij} of the structural stiffness matrix $[K]_{4\times4}$ and mass matrix $[M]_{4\times4}$ are described below:

$$\begin{aligned} &k_{11} = -\alpha^2 A_{11} - \beta^2 A_{66};\ k_{12} = -\alpha\beta\left(A_{12} + A_{66}\right); \\ &k_{13} = \alpha^3 B_{11} + \alpha\beta^2\left(B_{12} + 2B_{66}\right);\ k_{14} = 0;\ k_{22} = -\alpha^2 A_{66} - \beta^2 A_{22}; \\ &k_{23} = \alpha^2\beta\left(B_{12} + 2B_{66}\right) + \beta^3 B_{22};\ k_{24} = 0; \\ &k_{33} = -\alpha^4 D_{11} - 2\alpha^2\beta^2\left(D_{12} + 2D_{66}\right) - \beta^4 D_{22} - K_1 - K_2\left(\alpha^2 + \beta^2\right); \\ &k_{34} = -K_1 - K_2\left(\alpha^2 + \beta^2\right);\ k_{44} = -\alpha^2 A_{55}^s - \beta^2 A_{44}^s - K_1 - K_2\left(\alpha^2 + \beta^2\right); \\ &m_{11} = m_{22} = I_0;\ m_{13} = -I_1\alpha;\ m_{12} = m_{14} = 0;\ m_{23} = -I_1\beta;\ m_{24} = 0; \\ &m_{31} = -I_1\alpha;\ m_{33} = I_0 + I_2\left(\alpha^2 + \beta^2\right);\ m_{34} = I_0;\ m_{44} = I_0. \end{aligned} \tag{23}$$

in which for Winkler foundation: $K_1 = k_{\mathrm{w}};\ K_2 = 0$; for Pasternak foundation: $K_1 = k_{\mathrm{w}};\ K_2 = k_p$; for Kerr foundation: $K_1 = \left(k_l k_u\right)/\left(k_l + k_u\right);\ K_2 = \left(k_s k_u\right)/\left(k_l + k_u\right)$.

The fundamental natural frequency of the SAFGP plate placed on an elastic foundation was determined by solving the eigenvalue equation $\left|[K]_{4\times4} - \omega^2 [M]_{4\times4}\right| = 0$. The solution of this equation was the natural frequency ω_{mn} corresponding to the vibration mode (m, n). The fundamental natural frequency was then determined by: ω = $\min\{\omega_{mn}\}$.

Methodology Flowchart

To clarify the analytical procedure, a methodological flowchart is presented to illustrate the sequential steps of the study (**Figure 2**). The flow starts with the formulation of displacement fields using the four-variable HSDT theory, followed by the derivation of strain-displacement relations and stress-strain laws. Subsequently, the internal force resultants are obtained and incorporated into Hamilton's principle to establish the governing equations. The system of equations is then solved using the Navier method for simply supported boundary conditions. Finally, the eigenvalue problem is formulated and solved to obtain the natural frequencies. This structured approach ensures transparency and reproducibility in the vibration analysis of SAFGP plates.

Results and Discussion

Verification example

Two comparison examples were performed to verify the accuracy of the present model. The first comparison was carried out on an auxetic honeycomb core sandwich plate with isotropic surface layer (E= 69 GPa, ν = 0.33, ρ = 2700 kg m^{-3}). The comparison was done with the results of Tran *et al.* (2020) using a finite element model based on first-order shear deformation theory, as shown in **Table 1**.

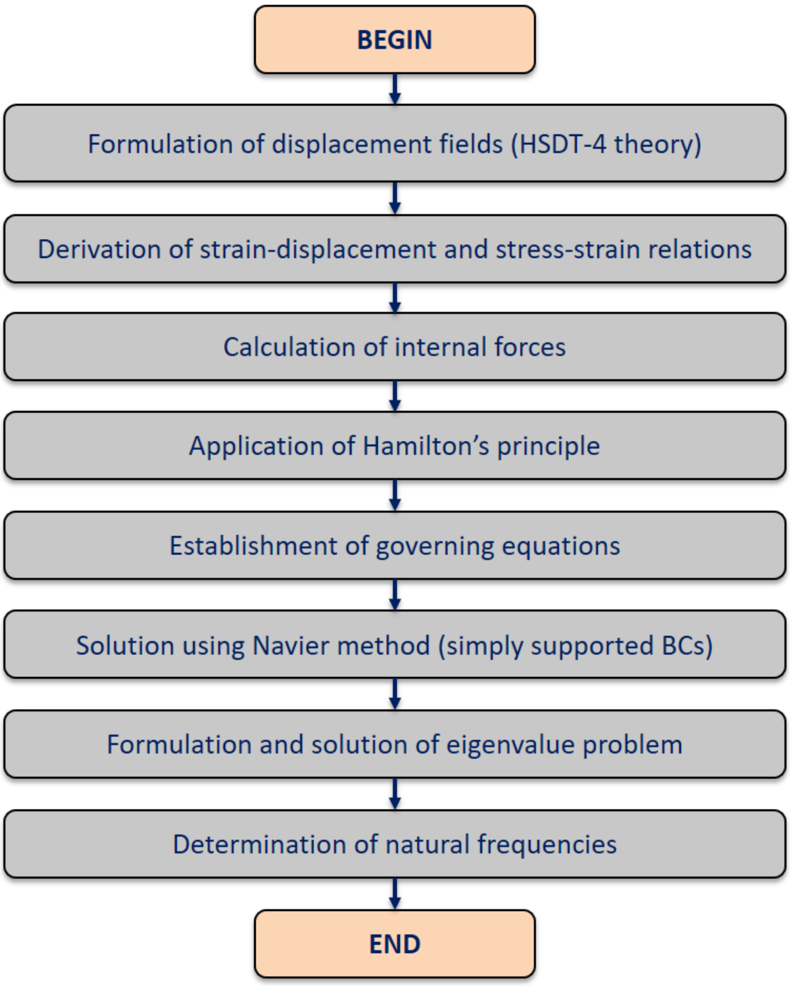

Figure 2. Methodology flowchart for free vibration analysis of SAFGP Plates

Table 1. Comparison of fundamental frequency of sandwich plates with isotropic surface layer, auxetic core on Pasternak elastic foundation (h = 0.1m; $a = b = 20h$; η_3= 0.01385, K_1 = 0.1 GPa/m; K_2 = 0.05 GPa.m)

θ	$\eta_1 = 0.5$		$\eta_1 = 2$		$\eta_1 = 4$	
	Present	Tran *et al.* (2020)	Present	Tran *et al.* (2020)	Present	Tran *et al.* (2020)
$\theta = 10^o$	276.5425	277.6223	280.3869	281.5118	280.8357	281.9645
$\theta = 35^o$	317.7951	319.2125	279.5374	280.6563	280.4536	281.5723
$\theta = 55^o$	292.4153	293.6156	277.8031	278.9102	279.6449	280.7500
$\theta = 80^o$	306.3131	307.5683	266.8752	267.9027	274.0952	275.1136

The second comparison was carried out for porous FGM (Al/Al_2O_3) sandwich plates. **Table 2** compares calculated dimensionless frequencies $\bar{\omega} = \omega a^2 / h\sqrt{\rho_0/E_0}$ ($\rho_0 =$ 1 GPa; E_0 =1 kg m^{-3}) with those of Daikh & Zenkour (2019) who employed a five-unknown displacement high-order plate theory (TSDT) and analytical solution. The results showed that, with different values of porosity coefficients, porosity distribution patterns, and core-to-face layers thickness ratios, the difference between the obtained were negligible.

Based on the two verification examples above, it can be concluded that the analytical model and computational program developed in this study were reliable. On that basis, parametric study was then carried out in the next section.

Parametric study

In this section, the free vibration analysis of a rectangular SAFGP plate (**Figure 1**) resting on a Winkler/Pasternak/Kerr elastic foundation is presented. The auxetic core material was made of isotropic material with the following parameters: elastic modulus E = 70 GPa, Poisson's ratio ν = 0.3 and density ρ = 2702 kg m^{-3}. The surface layer was made of FGM (Al/Al_2O_3) with the following mechanical properties: Al_2O_3: E_c = 380 GPa ; ρ_c = 3800 kg m^{-3}; ν_c = 0.3 and Al: E_m = 70 Gpa ; ρ_m = 2702 kg m^{-3}; ν_m = 0.3. Three types of SAFGP plates were considered: SAFGP-0 plates were made up of auxetic core and perfect FGM face sheets (without porosity, α_0=0); SAFGP-I plates were made up of auxetic core and FGM-I face sheets. SAFGP-II plates were made up of auxetic core and FGM-II face sheets.

Effect of elastic foundation

Table 3 reveals a key trend: the fundamental frequency of all three SAFGP plate types was consistently higher when placed on Pasternak or Kerr foundations as compared to the Winkler foundation. Mechanically, this indicated that the Winkler foundation exhibited significantly lower overall stiffness than the other two models. This difference arose because the Pasternak and Kerr foundations incorporated shear stiffness (k_p), which enhanced system rigidity. Notably, when the lower layer's bending stiffness and shear stiffness parameters were held constant, the plate's fundamental frequency on the Kerr foundation remained slightly lower than that on the Pasternak foundation.

From a mechanical perspective, this difference stemmed from the Kerr foundation model's inclusion of an additional elastic layer (k_l) in direct contact with the plate. This sub-layer behaved like a spring, effectively reducing the overall bending stiffness of the plate-foundation system compared to simpler foundation models. Furthermore, among the two types of plates with porous functionally graded surface layers, the SAFGP-II plate consistently exhibited a higher fundamental frequency than the SAFGP-I plate.

Influence of surface layer material properties

Table 4 and **Figure 3** show the variation of the fundamental natural frequency for the SAFGP plate with the change of the volume fraction index p and the porosity coefficient α_0, investigated for both types of surface layer pore distributions, FGM-I and FGM-II. The results show that the frequency tended to decrease as the

Table 2. Comparison of dimensionless fundamental natural frequencies of porous FGM sandwich plates (*p = 2; a/b = 1; a/h =10*)

Distribution type	α_0	Model	1-0-1	1-1-1	1-2-1	2-1-2
PB-I	0	Daikh & Zenkour (2019)	1.06155	1.18847	1.30244	1.12248
		Present	1.06215	1.18910	1.30351	1.12298
	0.1	T Daikh & Zenkour (2019)	0.98258	1.12071	1.24933	1.04712
		Present	0.99178	1.13005	1.25790	1.05662
	0.2	Daikh & Zenkour (2019)	0.87867	1.04201	1.19156	0.95491
		Present	0.89387	1.05744	1.20512	0.97081
PB-II	0.1	Daikh & Zenkour (2019)	1.03235	1.15768	1.27723	1.09008
		Present	1.03751	1.16294	1.28221	1.09542
	0.2	Daikh& Zenkour (2019)	1.00033	1.12524	1.25140	1.05528
		Present	1.00918	1.13416	1.25939	1.06451

Table 3. Fundamental natural frequency of SAFGP sandwich plates on elastic foundation (h = 0.1m; a = b = 20h; α_0 = 0.1; p = 5; η_1 = 2; η_3 = 0.01385; 1-2-1)

Foundation	Foundation coefficients	θ	SAFGP-0	SAFGP-I	SAFGP-II
Winkler	k_w = 0.1 GPa/m	10	223.037	218.429	221.042
		30	222.438	217.770	220.414
		45	221.540	216.782	219.473
		60	219.718	214.782	217.564
Pasternak	k_w = 0.1 GPa/m k_s = 0.05 GPa.m	10	303.605	308.941	306.244
		30	302.787	308.004	305.370
		45	301.559	306.601	304.060
		60	299.068	303.759	301.403
Kerr	k_u = k_l = 0.1 GPa/m k_s = 0.05 GPa.m	10	249.725	248.808	249.437
		30	249.053	248.055	248.727
		45	248.046	246.928	247.662
		60	246.002	244.645	245.504

Table 4. Fundamental frequency of SAFGP plates as a function of p and α_0 (h = 0.1m; a = b = 20h; α_0 = 0.1; η_1 = 1; η_3 = 0.01385; 1-2-1; k_u = k_l = k_s = 0)

Porosity distribution	α_0	p				
		0.2	1	2	5	10
FGM-I	0	323.334	285.687	266.291	248.589	241.909
	0.05	326.089	287.100	266.795	248.096	240.988
	0.1	329.085	288.656	267.354	247.535	239.939
	0.15	332.353	290.380	267.976	246.891	238.733
	0.2	335.934	292.299	268.672	246.143	237.330
FGM-II	0	323.334	285.687	266.291	248.589	241.909
	0.05	324.724	286.429	266.596	248.418	241.535
	0.1	326.172	287.206	266.917	248.236	241.136
	0.15	327.681	288.022	267.255	248.041	240.711
	0.2	329.256	288.879	267.611	247.833	240.256

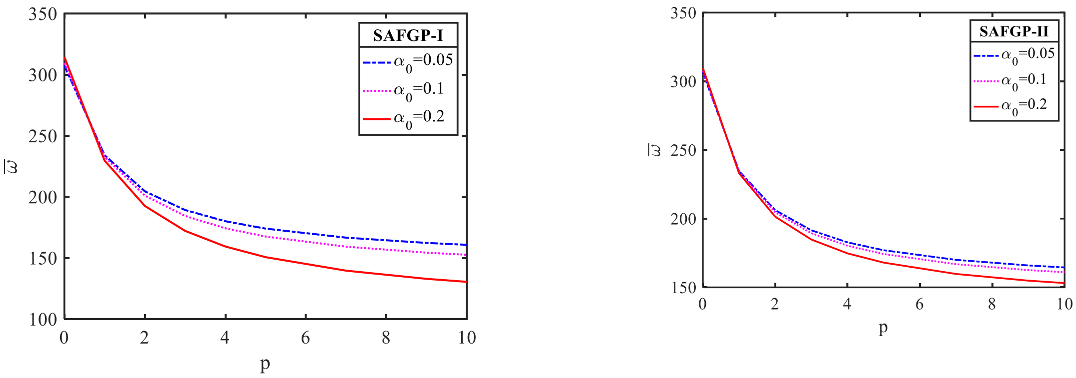

a) SAFGP-I b) SAFGP-II

Figure 3. Variation of dimensionless fundamental frequency of SAFGP plates as a function of p (h = 0.1m; $a = b = 20h$; α_0 = 0.1; θ = 10; η_1 = 1; η_3 = 0.01385; 1-2-1; $k_u = k_l = k_s$=0)

p index increased. This phenomenon could be explained by the change in material composition: as p increased, the metal (Al) ratio in the FGM material increasedwhile the ceramic (Al_2O_3) component decreased. Since the elastic modulus of metal (E_m = 70 GPa) was much lower than that of ceramic (E_c = 380 GPa), this change in composition led to a decrease in the overall stiffness of the plate and consequently a decrease in the frequency. On the other hand, the results from the graph also demonstrate that the porosity coefficient α_0 showed a clear influence on the frequency. Specifically, the frequency decreased significantly when α_0 increased. In terms of mechanical standpoint, the increase in porosity changed the mechanical properties of the material, especially reducing the effective modulus of elasticity, thereby leading to a decrease in the overall stiffness of the plate.

Influence of the properties of auxetic core material

In this section, the influence of the geometric parameters of the auxetic unit cell on the fundamental natural frequency of the SAFGP plate were analyzed in detail. First, **Figure 4** shows the influence of the inclined angle θ on the fundamental frequency of the plate (η_1 changes and η_3= 0.01385). For the case of η_1 = 1, the fundamental frequency decreased significantly as the angle θ increased, and according to the geometrical characteristics of the auxetic unit cell, the value of θ cannot exceed 30° when η_1 = 1. For the values of η_1 = 2, 3, and 5, as θ increased, the fundamental frequency of the plate continued to decrease in a similar trend, and the rate of decrease became more obvious when $\theta \geq 30°$.

In order to further analyze the influence of the geometric parameters of the auxetic unit cell, **Figure 5** shows the impact of the two parameters η_1 and η_3 on the fundamental natural frequency of the SAFGP plate. The results demonstrate that when the parameter η_3 increased, the fundamental frequency tended to decrease, while increasing η_1 increased the frequency, which means improving the stiffness of the plate. Thus, the two parameters η_1 and η_3 affected the stiffness of the structure in opposite directions, thereby providing an important basis for optimizing the design of SAFGP plates in practical applications.

Influence of sandwich plate structure

Table 5 presents the results of the fundamental frequency analysis of two types of SAFGP-I and SAFGP-II plates placed on Kerr elastic foundation with five face-to-core thickness ratios (1-1-1, 1-2-1, 1-3-1, 1-4-1 and 2-1-2). The results show three main trends: the fundamental frequency increased with increasing auxetic core layer thickness; the fundamental frequency decreased with increasing α_0 coefficient and inclined angle θ; SAFGP plates with FGM-II surface layer always gave higher frequencies than FGM-I. Notably, these trends are completely consistent with the results obtained for the case of plates not placed on Kerr elastic foundation, demonstrating that the influence of material parameters (α_0, θ) and structure (layer thickness ratio, porosity distribution pattern) on the vibration behavior is similar in both cases with and without elastic foundation.

Effect of plate's geometric parameters

Figure 6 illustrates the effect of the side-to-thichkenss ratio *a/h* and aspect ratio *b/a* on the dimensionless fundamental natural frequency of the SPoFGM sandwich plates, where *a* is fixed as 1m, while *h* and *b* are varied. The results show that as the ratio *b/a* increased, the frequencies of both SAFGP-I and SAFGP-II plates decreased. This was consistent with the trend because as the ratio *b*/*a* increased, the geometry of the plate became more elongated in the transverse direction, allowing greater deformation along the wider side. This change reduced the effective stiffness-to-mass ratio of the plate, resulting in a decrease in the dimensionless frequency. On the other hand, when keeping *a* = 1m fixed and increasing the ratio *a/h* (i.e. decreasing the thickness *h*), the frequency of the plate also tended to decrease. The reason was that the decrease in thickness reduced the stiffness of the plate, leading to a lower frequency.

Limitations of the Study

While the current analytical model provided valuable insights into the free vibration characteristics of SAFGP plates resting on

Table 5. Fundamental frequency of SAFGP plates as a function of thickness ratio (h = 0.1m; $a = b$ = 20h; α_0 = 0.1; p = 5; η_1 = 2; η_3 = 0.01385; $k_u = k_l$ = 0.1 GPa/m; k_s = 0.05 GPa.m)

Porosity distribution	α_0	θ	1-1-1	1-2-1	1-3-1	1-4-1	2-1-2
FGM-I	0.1	10	215.557	248.808	273.677	293.645	194.083
		30	215.227	248.055	272.450	291.911	193.933
		45	214.729	246.928	270.624	289.342	193.706
		60	213.710	244.645	266.960	284.241	193.240
FGM-II		10	217.033	249.437	273.581	292.901	196.063
		30	216.720	248.727	272.427	291.272	195.921
		45	216.248	247.662	270.705	288.855	195.705
		60	215.282	245.504	267.248	284.044	195.262
FGM-I	0.2	10	212.622	247.590	274.076	295.531	190.323
		30	212.249	246.735	272.674	293.541	190.155
		45	211.688	245.455	270.591	290.603	189.900
		60	210.541	242.870	266.431	284.799	189.378
FGM-II		10	216.179	249.107	273.849	293.755	195.082
		30	215.847	248.354	272.622	292.021	194.931
		45	215.348	247.225	270.794	289.451	194.703
		60	214.326	244.939	267.129	284.347	194.235

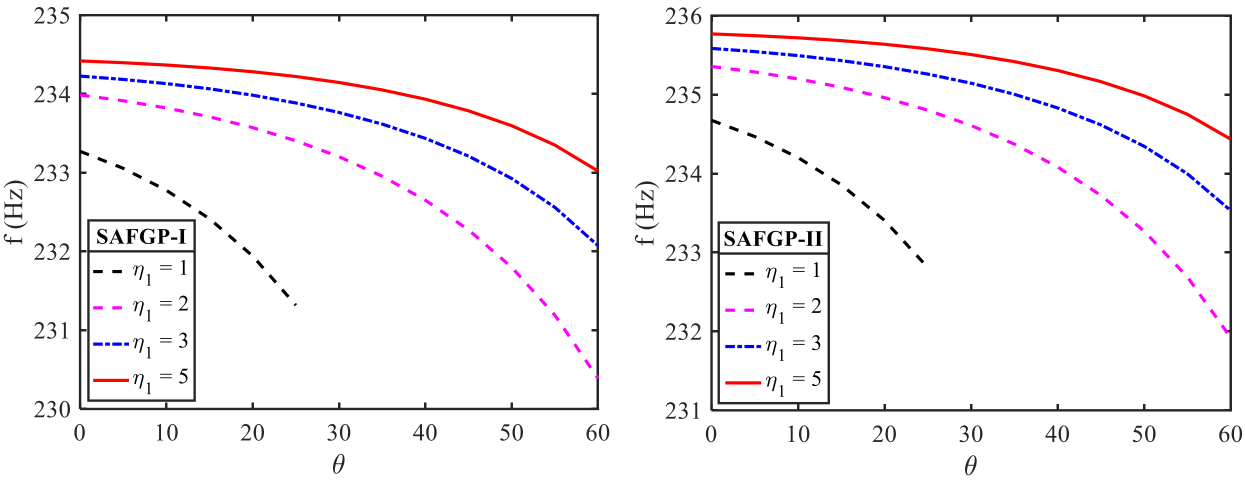

(a) SAFGP-I (b) SAFGP-II

Figure 4. Variation of fundamental frequency of SAFGP plates as a function of inclined angle θ (h = 0.1m; a = b = 20h; α_0 = 0.1; p = 1; η_3 = 0.01385; 1-2-1)

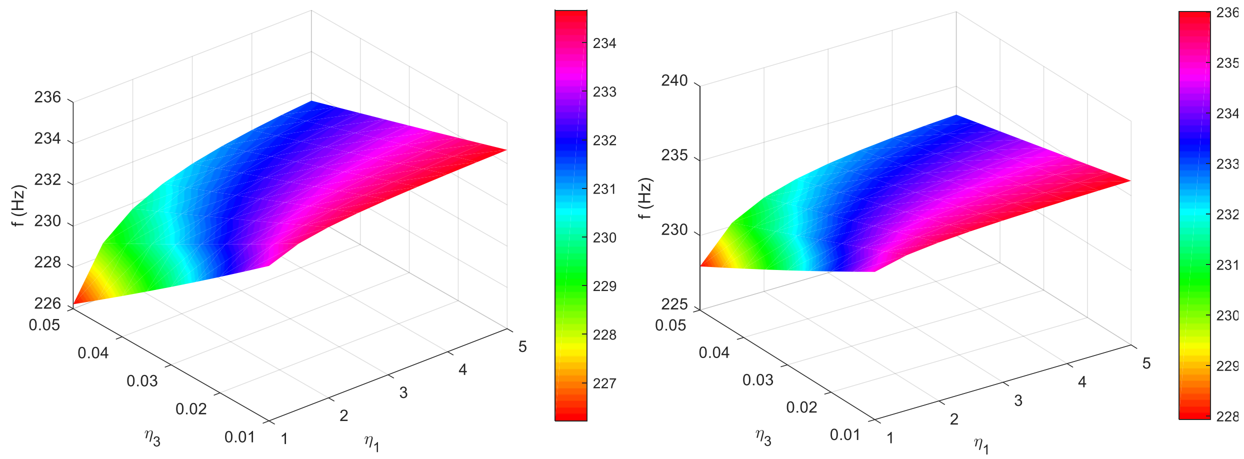

a) SAFGP-I b) SAFGP-II

Figure 5. Variation of fundamental frequency as a function of η_1 and η_3 (h = 0.1m; a = b = 20h; α_0 = 0.1; p = 1; θ = *10;* 1-2-1)

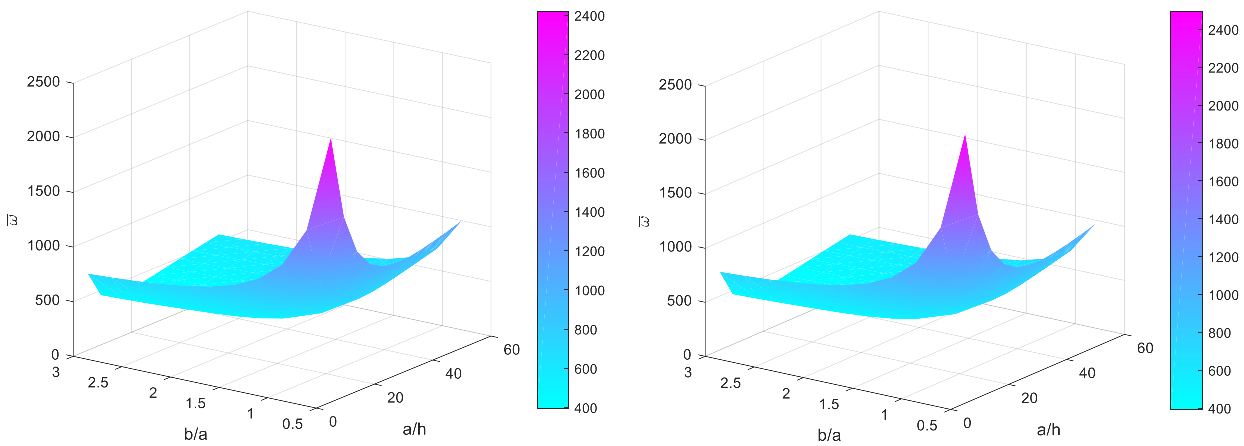

a) SAFGP-I b) SAFGP-II

Figure 6. Variation of dimensionless fundamental frequency of SAFGP plates as a function of *a/h* and *b/a* ratios (a = *1m*; α_0 = 0.1; p = 5; θ = *10;* η_1 = 2; η_3 = 0.01385; k_u = k_l = 0.1 GPa/m; k_s = 0.05 GPa.m, 1-2-1)

various elastic foundations, some limitations remain. First, the model assumed ideal boundary conditions (simply supported), which may differ from practical applications where boundary constraints are more complex. Second, the analysis neglected damping effects, which are important in dynamic responses. Third, temperature-dependent material properties were not considered, even though they could significantly influence the behavior of FGM-based structures. Future research should address these aspects to further enhance the applicability of the proposed model in real-world engineering systems.

Conclusions

The paper presents a theoretical study of the free vibration of porous sandwich plates with auxetic core and FGM surface layer placed on Winkler/Pasternak/Kerr elastic foundation, using the four-unknown displacement high-order shear deformation theory. Two types of porosity distribution in the surface layer were investigated. The verification of fundamental frequency with available literature confirms the reliability of the proposed theoretical model. The study has drawn some important conclusions:

(i) The porosity distribution strongly affects the vibrational characteristics of the plate, which is shown by the difference in frequency between the two distribution types FGM-I and FGM-II.

(ii) The geometric parameters of the auxetic core (η_1, η_3, θ) together with the core thickness affect the fundamental frequency: the frequency decreases when η_3 and the inclined angle θ increase, conversely, the frequency increases when η_1 and the core thickness increase.

(iii) The research results show that the presence of elastic foundation has a significant influence on the fundamental frequency.

(iv) The geometric ratios (b/a and a/h) strongly influence the frequency: as these ratios increase, the overall stiffness of the structure decreases, leading to a decrease in the frequency.

These findings provide an important scientific basis for the design and optimization of auxetic-FGM sandwich structures in engineering applications, especially in dynamically loaded systems. Furthermore, since no available FEM software currently supports this type of complex sandwich structure with auxetic core and porous FGM layers on Winkler/Pasternak/Kerr foundations, the present results serve as valuable benchmark data for future analytical and numerical developments.

References

Ait Atmane H., Tounsi A. & Bernard F. (2017). Effect of thickness stretching and porosity on mechanical response of a functionally graded beams resting on elastic foundations. International Journal of Mechanics and Materials in Design. 13: 71-84.

Alderson A. & Evans K. (1995). Microstructural modelling of auxetic microporous polymers. Journal of Materials Science. 30(13): 3319-3332.

Alibeigloo A. & Alizadeh. M. (2015). Static and free vibration analyses of functionally graded sandwich plates using state space differential quadrature method. European Journal of Mechanics-A/Solids. 54: 252-266.

Bohara R. P. , Linforth S., Nguyen T., Ghazlan A. & Ngo T. (2023). Anti-blast and-impact performances of auxetic structures: A review of structures, materials, methods, and fabrications. Engineering structures. 276: 115377.

Daikh A. A. & Zenkour A. M. (2019). Free vibration and buckling of porous power-law and sigmoid functionally graded sandwich plates using a simple higher-order shear deformation theory. Materials Research Express. 6(11): 115707.

Ghazwani M. H., Alnujaie A. & Vinh P. V. (2024). A general viscoelastic foundation model for vibration analysis of functionally graded sandwich plate with auxetic core. Defence Technology. 46: 40-58.

Houari M. S. A., Tounsi A. & Bég O. A. (2013). Thermoelastic bending analysis of functionally graded sandwich plates using a new higher order shear and normal deformation theory. International Journal of Mechanical Sciences. 76: 102-111.

Imbalzano G., Tran P., Ngo T. D. & Lee P. V. S. (2016). A numerical study of auxetic composite panels under blast loadings. Composite Structures. 135: 339-352.

Kerr A. D. (1965). A study of a new foundation model. Acta Mechanica. 1(2): 135-147.

Kerr A. D. (1984). On the formal development of elastic foundation models. Ingenieur-Archiv. 54(6): 455-464.

Kumar P. & Harsha S. (2022). Static analysis of porous core functionally graded piezoelectric (PCFGP) sandwich plate resting on the Winkler/Pasternak/Kerr foundation under thermo-electric effect. Materials Today Communications. 32: 103929.

Le Thanh Hai, Nguyen Van Long & Tran Minh Tu (2024). Free vibration and dynamic response of functionally graded plates with porosities resting on Kerr's elastic foundation. Journal of Science and Technology in Civil Engineering (JSTCE). 18(3V): 1-15 (in Vietnamese).

Li M., Soares C. G. & Yan R. (2021). Free vibration analysis of FGM plates on Winkler/Pasternak/Kerr foundation by using a simple quasi-3D HSDT. Composite Structures. 264: 113643.

Li Q., Iu V. & Kou K. (2008). Three-dimensional vibration analysis of functionally graded material sandwich plates. Journal of Sound and Vibration. 311(1-2): 498-515.

Liang C. & Wang Y. Q. (2020). A quasi-3D trigonometric shear deformation theory for wave propagation analysis of FGM sandwich plates with porosities resting on viscoelastic foundation. Composite Structures. 247: 112478.

Merdaci S., Adda H. M., Hakima B., Dimitri R. & Tornabene F. (2021). Higher-order free vibration analysis of porous functionally graded plates. Journal of Composites Science. 5(11): 305.

Nguyen N. V, Nguyen X. H., Nguyen N. T., Kang J. & Lee J. (2021). A comprehensive analysis of auxetic honeycomb sandwich plates with graphene nanoplatelets reinforcement. Composite Structures. 259: 113213.

Pasternak P. (1954). On a new method of analysis of an elastic foundation by means of two foundation constants. Gosudarstvennoe Izdatelstro Liberaturi po Stroitelstvui Arkhitekture, Moscow.

Quoc T. H., Tu T. M. & Tham V. V. (2019). Free vibration analysis of smart laminated functionally graded CNT reinforced composite plates via new four-variable refined plate theory. Materials. 12(22): 3675.

Quoc T. H., Tham V. V., Long N. V. & Tu T. M. (2023). Free vibration and nonlinear dynamic response of sandwich plates with auxetic honeycomb core and piezoelectric face sheets. Thin-Walled Structures. 191: 111141.

Reddy J. (2000). Analysis of functionally graded plates. International Journal for numerical methods in engineering. 47(1-3): 663-684.

Shahsavari D., Shahsavari M., Li L. & Karami B. (2018). A novel quasi-3D hyperbolic theory for free vibration of FG plates with porosities resting on Winkler/Pasternak/Kerr foundation. Aerospace Science and Technology. 72: 134-149.

Thai H. T., Nguyen T. K., Vo P. T. & Lee J. (2014). Analysis of functionally graded sandwich plates using a new first-order shear deformation theory. European Journal of Mechanics-A/Solids. 45: 211-225.

Tran T. T., Pham Q. H., Thoi T. N. & Tran V. T. (2020). Dynamic analysis of sandwich auxetic honeycomb plates subjected to moving oscillator load on elastic foundation. Advances in Materials Science and Engineering. DOI: 10.1155/2020/6309130.

Vu Van Tham, Vu Minh Ngoc & Pham Trong Khoi (2024). Static analysis of sandwich curved FG porous beams resting on Winkler/Pasternak/Kerr foundation. Journal of Science and Technology in Civil Engineering (JSTCE). 18(3V): 48-63 (in Vietnamese).

Vu Van Tham (2025). Vibration characteristics of functionally graded magneto-electro-elastic plates with porosities resting on Kerr's elastic foundation. Journal of Science and Technology in Civil Engineering (JSTCE). 19(1V): 134-151 (in Vietnamese).

Winkler E. (1867). Die Lehre von der Elasticitaet und Festigkeit: mit besonderer Rücksicht auf ihre Anwendung in der Technik, für polytechnische Schulen, Bauakademien, Ingenieure, Maschinenbauer, Architecten, etc. H. Dominicus (German Edition).

Yousfi M., Ait A. H., Meradjah M., Tounsi A. & Bennai R. (2018). Free vibration of FGM plates with porosity by a shear deformation theory with four variables. Structural engineering and mechanics: An international journal. 66(3): 353-368.

Zenkour A. (2005a). A comprehensive analysis of functionally graded sandwich plates: Part 1 - Deflection and stresses. International journal of solids and structures. 42(18-19): 5224-5242.

Zenkour A. (2005b). A comprehensive analysis of functionally graded sandwich plates: Part 2—Buckling and free vibration. International Journal of Solids and Structures. 42(18-19): 5243-5258.

Zenkour A. M. (2006). Generalized shear deformation theory for bending analysis of functionally graded plates. Applied Mathematical Modelling. 30(1): 67-84.

Zhao X. Y. L. & Liew K. M. (2009). Free vibration analysis of functionally graded plates using the element-free kp-Ritz method. Journal of sound and Vibration. 319(3-5): 918-939.